Direct Limits on the B_s^0 Oscillation Frequency

V.M. Abazov,[36] B. Abbott,[76] M. Abolins,[66] B.S. Acharya,[29] M. Adams,[52] T. Adams,[50] M. Agelou,[18] J.-L. Agram,[19] S.H. Ahn,[31] M. Ahsan,[60] G.D. Alexeev,[36] G. Alkhazov,[40] A. Alton,[65] G. Alverson,[64] G.A. Alves,[2] M. Anastasoaie,[35] T. Andeen,[54] S. Anderson,[46] B. Andrieu,[17] M.S. Anzelc,[54] Y. Arnoud,[14] M. Arov,[53] A. Askew,[50] B. Åsman,[41] A.C.S. Assis Jesus,[3] O. Atramentov,[58] C. Autermann,[21] C. Avila,[8] C. Ay,[24] F. Badaud,[13] A. Baden,[62] L. Bagby,[53] B. Baldin,[51] D.V. Bandurin,[36] P. Banerjee,[29] S. Banerjee,[29] E. Barberis,[64] P. Bargassa,[81] P. Baringer,[59] C. Barnes,[44] J. Barreto,[2] J.F. Bartlett,[51] U. Bassler,[17] D. Bauer,[44] A. Bean,[59] M. Begalli,[3] M. Begel,[72] C. Belanger-Champagne,[5] A. Bellavance,[68] J.A. Benitez,[66] S.B. Beri,[27] G. Bernardi,[17] R. Bernhard,[42] L. Berntzon,[15] I. Bertram,[43] M. Besançon,[18] R. Beuselinck,[44] V.A. Bezzubov,[39] P.C. Bhat,[51] V. Bhatnagar,[27] M. Binder,[25] C. Biscarat,[43] K.M. Black,[63] I. Blackler,[44] G. Blazey,[53] F. Blekman,[44] S. Blessing,[50] D. Bloch,[19] K. Bloom,[68] U. Blumenschein,[23] A. Boehnlein,[51] O. Boeriu,[56] T.A. Bolton,[60] F. Borcherding,[51] G. Borissov,[43] K. Bos,[34] T. Bose,[78] A. Brandt,[79] R. Brock,[66] G. Brooijmans,[71] A. Bross,[51] D. Brown,[79] N.J. Buchanan,[50] D. Buchholz,[54] M. Buehler,[82] V. Buescher,[23] S. Burdin,[51] S. Burke,[46] T.H. Burnett,[83] E. Busato,[17] C.P. Buszello,[44] J.M. Butler,[63] S. Calvet,[15] J. Cammin,[72] S. Caron,[34] W. Carvalho,[3] B.C.K. Casey,[78] N.M. Cason,[56] H. Castilla-Valdez,[33] S. Chakrabarti,[29] D. Chakraborty,[53] K.M. Chan,[72] A. Chandra,[49] D. Chapin,[78] F. Charles,[19] E. Cheu,[46] F. Chevallier,[14] D.K. Cho,[63] S. Choi,[32] B. Choudhary,[28] L. Christofek,[59] D. Claes,[68] B. Clément,[19] C. Clément,[41] Y. Coadou,[5] M. Cooke,[81] W.E. Cooper,[51] D. Coppage,[59] M. Corcoran,[81] M.-C. Cousinou,[15] B. Cox,[45] S. Crépé-Renaudin,[14] D. Cutts,[78] M. Ćwiok,[30] H. da Motta,[2] A. Das,[63] M. Das,[61] B. Davies,[43] G. Davies,[44] G.A. Davis,[54] K. De,[79] P. de Jong,[34] S.J. de Jong,[35] E. De La Cruz-Burelo,[65] C. De Oliveira Martins,[3] J.D. Degenhardt,[65] F. Déliot,[18] M. Demarteau,[51] R. Demina,[72] P. Demine,[18] D. Denisov,[51] S.P. Denisov,[39] S. Desai,[73] H.T. Diehl,[51] M. Diesburg,[51] M. Doidge,[43] A. Dominguez,[68] H. Dong,[73] L.V. Dudko,[38] L. Duflot,[16] S.R. Dugad,[29] A. Duperrin,[15] J. Dyer,[66] A. Dyshkant,[53] M. Eads,[68] D. Edmunds,[66] T. Edwards,[45] J. Ellison,[49] J. Elmsheuser,[25] V.D. Elvira,[51] S. Eno,[62] P. Ermolov,[38] J. Estrada,[51] H. Evans,[55] A. Evdokimov,[37] V.N. Evdokimov,[39] S.N. Fatakia,[63] L. Feligioni,[63] A.V. Ferapontov,[60] T. Ferbel,[72] F. Fiedler,[25] F. Filthaut,[35] W. Fisher,[51] H.E. Fisk,[51] I. Fleck,[23] M. Ford,[45] M. Fortner,[53] H. Fox,[23] S. Fu,[51] S. Fuess,[51] T. Gadfort,[83] C.F. Galea,[35] E. Gallas,[51] E. Galyaev,[56] C. Garcia,[72] A. Garcia-Bellido,[83] J. Gardner,[59] V. Gavrilov,[37] A. Gay,[19] P. Gay,[13] D. Gelé,[19] R. Gelhaus,[49] C.E. Gerber,[52] Y. Gershtein,[50] D. Gillberg,[5] G. Ginther,[72] N. Gollub,[41] B. Gómez,[8] K. Gounder,[51] A. Goussiou,[56] P.D. Grannis,[73] H. Greenlee,[51] Z.D. Greenwood,[61] E.M. Gregores,[4] G. Grenier,[20] Ph. Gris,[13] J.-F. Grivaz,[16] S. Grünendahl,[51] M.W. Grünewald,[30] F. Guo,[73] J. Guo,[73] G. Gutierrez,[51] P. Gutierrez,[76] A. Haas,[71] N.J. Hadley,[62] P. Haefner,[25] S. Hagopian,[50] J. Haley,[69] I. Hall,[76] R.E. Hall,[48] L. Han,[7] K. Hanagaki,[51] K. Harder,[60] A. Harel,[72] R. Harrington,[64] J.M. Hauptman,[58] R. Hauser,[66] J. Hays,[54] T. Hebbeker,[21] D. Hedin,[53] J.G. Hegeman,[34] J.M. Heinmiller,[52] A.P. Heinson,[49] U. Heintz,[63] C. Hensel,[59] G. Hesketh,[64] M.D. Hildreth,[56] R. Hirosky,[82] J.D. Hobbs,[73] B. Hoeneisen,[12] M. Hohlfeld,[16] S.J. Hong,[31] R. Hooper,[78] P. Houben,[34] Y. Hu,[73] V. Hynek,[9] I. Iashvili,[70] R. Illingworth,[51] A.S. Ito,[51] S. Jabeen,[63] M. Jaffré,[16] S. Jain,[76] V. Jain,[74] K. Jakobs,[23] C. Jarvis,[62] A. Jenkins,[44] R. Jesik,[44] K. Johns,[46] C. Johnson,[71] M. Johnson,[51] A. Jonckheere,[51] P. Jonsson,[44] A. Juste,[51] D. Käfer,[21] S. Kahn,[74] E. Kajfasz,[15] A.M. Kalinin,[36] J.M. Kalk,[61] J.R. Kalk,[66] S. Kappler,[21] D. Karmanov,[38] J. Kasper,[63] I. Katsanos,[71] D. Kau,[50] R. Kaur,[27] R. Kehoe,[80] S. Kermiche,[15] S. Kesisoglou,[78] A. Khanov,[77] A. Kharchilava,[70] Y.M. Kharzheev,[36] D. Khatidze,[71] H. Kim,[79] T.J. Kim,[31] M.H. Kirby,[35] B. Klima,[51] J.M. Kohli,[27] J.-P. Konrath,[23] M. Kopal,[76] V.M. Korablev,[39] J. Kotcher,[74] B. Kothari,[71] A. Koubarovsky,[38] A.V. Kozelov,[39] J. Kozminski,[66] A. Kryemadhi,[82] S. Krzywdzinski,[51] T. Kuhl,[24] A. Kumar,[70] S. Kunori,[62] A. Kupco,[11] T. Kurča,[20,*] J. Kvita,[9] S. Lager,[41] S. Lammers,[71] G. Landsberg,[78] J. Lazoflores,[50] A.-C. Le Bihan,[19] P. Lebrun,[20] W.M. Lee,[53] A. Leflat,[38] F. Lehner,[42] C. Leonidopoulos,[71] V. Lesne,[13] J. Leveque,[46] P. Lewis,[44] J. Li,[79] Q.Z. Li,[51] J.G.R. Lima,[53] D. Lincoln,[51] J. Linnemann,[66] V.V. Lipaev,[39] R. Lipton,[51] Z. Liu,[5] L. Lobo,[44] A. Lobodenko,[40] M. Lokajicek,[11] A. Lounis,[19] P. Love,[43] H.J. Lubatti,[83] M. Lynker,[56] A.L. Lyon,[51] A.K.A. Maciel,[2] R.J. Madaras,[47] P. Mättig,[26] C. Magass,[21] A. Magerkurth,[65] A.-M. Magnan,[14] N. Makovec,[16] P.K. Mal,[56] H.B. Malbouisson,[3] S. Malik,[68] V.L. Malyshev,[36] H.S. Mao,[6] Y. Maravin,[60] M. Martens,[51] S.E.K. Mattingly,[78] R. McCarthy,[73] R. McCroskey,[46] D. Meder,[24] A. Melnitchouk,[67] A. Mendes,[15] L. Mendoza,[8] M. Merkin,[38] K.W. Merritt,[51] A. Meyer,[21] J. Meyer,[22] M. Michaut,[18] H. Miettinen,[81] T. Millet,[20] J. Mitrevski,[71] J. Molina,[3] N.K. Mondal,[29] J. Monk,[45] R.W. Moore,[5] T. Moulik,[59] G.S. Muanza,[16] M. Mulders,[51] M. Mulhearn,[71] L. Mundim,[3] Y.D. Mutaf,[73] E. Nagy,[15]

M. Naimuddin,[28] M. Narain,[63] N.A. Naumann,[35] H.A. Neal,[65] J.P. Negret,[8] S. Nelson,[50] P. Neustroev,[40]
C. Noeding,[23] A. Nomerotski,[51] S.F. Novaes,[4] T. Nunnemann,[25] V. O'Dell,[51] D.C. O'Neil,[5] G. Obrant,[40]
V. Oguri,[3] N. Oliveira,[3] N. Oshima,[51] R. Otec,[10] G.J. Otero y Garzón,[52] M. Owen,[45] P. Padley,[81] N. Parashar,[57]
S.-J. Park,[72] S.K. Park,[31] J. Parsons,[71] R. Partridge,[78] N. Parua,[73] A. Patwa,[74] G. Pawloski,[81] P.M. Perea,[49]
E. Perez,[18] K. Peters,[45] P. Pétroff,[16] M. Petteni,[44] R. Piegaia,[1] M.-A. Pleier,[22] P.L.M. Podesta-Lerma,[33]
V.M. Podstavkov,[51] Y. Pogorelov,[56] M.-E. Pol,[2] A. Pompoš,[76] B.G. Pope,[66] A.V. Popov,[39] W.L. Prado da Silva,[3]
H.B. Prosper,[50] S. Protopopescu,[74] J. Qian,[65] A. Quadt,[22] B. Quinn,[67] K.J. Rani,[29] K. Ranjan,[28] P.A. Rapidis,[51]
P.N. Ratoff,[43] P. Renkel,[80] S. Reucroft,[64] M. Rijssenbeek,[73] I. Ripp-Baudot,[19] F. Rizatdinova,[77] S. Robinson,[44]
R.F. Rodrigues,[3] C. Royon,[18] P. Rubinov,[51] R. Ruchti,[56] V.I. Rud,[38] G. Sajot,[14] A. Sánchez-Hernández,[33]
M.P. Sanders,[62] A. Santoro,[3] G. Savage,[51] L. Sawyer,[61] T. Scanlon,[44] D. Schaile,[25] R.D. Schamberger,[73]
Y. Scheglov,[40] H. Schellman,[54] P. Schieferdecker,[25] C. Schmitt,[26] C. Schwanenberger,[45] A. Schwartzman,[69]
R. Schwienhorst,[66] S. Sengupta,[50] H. Severini,[76] E. Shabalina,[52] M. Shamim,[60] V. Shary,[18] A.A. Shchukin,[39]
W.D. Shephard,[56] R.K. Shivpuri,[28] D. Shpakov,[64] V. Siccardi,[19] R.A. Sidwell,[60] V. Simak,[10] V. Sirotenko,[51]
P. Skubic,[76] P. Slattery,[72] R.P. Smith,[51] G.R. Snow,[68] J. Snow,[75] S. Snyder,[74] S. Söldner-Rembold,[45] X. Song,[53]
L. Sonnenschein,[17] A. Sopczak,[43] M. Sosebee,[79] K. Soustruznik,[9] M. Souza,[2] B. Spurlock,[79] J. Stark,[14] J. Steele,[61]
K. Stevenson,[55] V. Stolin,[37] A. Stone,[52] D.A. Stoyanova,[39] J. Strandberg,[41] M.A. Strang,[70] M. Strauss,[76]
R. Ströhmer,[25] D. Strom,[54] M. Strovink,[47] L. Stutte,[51] S. Sumowidagdo,[50] A. Sznajder,[3] M. Talby,[15]
P. Tamburello,[46] W. Taylor,[5] P. Telford,[45] J. Temple,[46] B. Tiller,[25] M. Titov,[23] V.V. Tokmenin,[36] M. Tomoto,[51]
T. Toole,[62] I. Torchiani,[23] S. Towers,[43] T. Trefzger,[24] S. Trincaz-Duvoid,[17] D. Tsybychev,[73] B. Tuchming,[18]
C. Tully,[69] A.S. Turcot,[45] P.M. Tuts,[71] R. Unalan,[66] L. Uvarov,[40] S. Uvarov,[40] S. Uzunyan,[53] B. Vachon,[5]
P.J. van den Berg,[34] R. Van Kooten,[55] W.M. van Leeuwen,[34] N. Varelas,[52] E.W. Varnes,[46] A. Vartapetian,[79]
I.A. Vasilyev,[39] M. Vaupel,[26] P. Verdier,[20] L.S. Vertogradov,[36] M. Verzocchi,[51] F. Villeneuve-Seguier,[44] P. Vint,[44]
J.-R. Vlimant,[17] E. Von Toerne,[60] M. Voutilainen,[68,†] M. Vreeswijk,[34] H.D. Wahl,[50] L. Wang,[62] J. Warchol,[56]
G. Watts,[83] M. Wayne,[56] M. Weber,[51] H. Weerts,[66] N. Wermes,[22] M. Wetstein,[62] A. White,[79] D. Wicke,[26]
G.W. Wilson,[59] S.J. Wimpenny,[49] M. Wobisch,[51] J. Womersley,[51] D.R. Wood,[64] T.R. Wyatt,[45] Y. Xie,[78]
N. Xuan,[56] S. Yacoob,[54] R. Yamada,[51] M. Yan,[62] T. Yasuda,[51] Y.A. Yatsunenko,[36] K. Yip,[74] H.D. Yoo,[78]
S.W. Youn,[54] C. Yu,[14] J. Yu,[79] A. Yurkewicz,[73] A. Zatserklyaniy,[53] C. Zeitnitz,[26] D. Zhang,[51] T. Zhao,[83]
Z. Zhao,[65] B. Zhou,[65] J. Zhu,[73] M. Zielinski,[72] D. Zieminska,[55] A. Zieminski,[55] V. Zutshi,[53] and E.G. Zverev[38]
(DØ Collaboration)
[1]*Universidad de Buenos Aires, Buenos Aires, Argentina*
[2]*LAFEX, Centro Brasileiro de Pesquisas Físicas, Rio de Janeiro, Brazil*
[3]*Universidade do Estado do Rio de Janeiro, Rio de Janeiro, Brazil*
[4]*Instituto de Física Teórica, Universidade Estadual Paulista, São Paulo, Brazil*
[5]*University of Alberta, Edmonton, Alberta, Canada, Simon Fraser University, Burnaby, British Columbia, Canada,
York University, Toronto, Ontario, Canada, and McGill University, Montreal, Quebec, Canada*
[6]*Institute of High Energy Physics, Beijing, People's Republic of China*
[7]*University of Science and Technology of China, Hefei, People's Republic of China*
[8]*Universidad de los Andes, Bogotá, Colombia*
[9]*Center for Particle Physics, Charles University, Prague, Czech Republic*
[10]*Czech Technical University, Prague, Czech Republic*
[11]*Center for Particle Physics, Institute of Physics, Academy of Sciences of the Czech Republic, Prague, Czech Republic*
[12]*Universidad San Francisco de Quito, Quito, Ecuador*
[13]*Laboratoire de Physique Corpusculaire, IN2P3-CNRS, Université Blaise Pascal, Clermont-Ferrand, France*
[14]*Laboratoire de Physique Subatomique et de Cosmologie, IN2P3-CNRS, Universite de Grenoble 1, Grenoble, France*
[15]*CPPM, IN2P3-CNRS, Université de la Méditerranée, Marseille, France*
[16]*IN2P3-CNRS, Laboratoire de l'Accélérateur Linéaire, Orsay, France*
[17]*LPNHE, IN2P3-CNRS, Universités Paris VI and VII, Paris, France*
[18]*DAPNIA/Service de Physique des Particules, CEA, Saclay, France*
[19]*IReS, IN2P3-CNRS, Université Louis Pasteur, Strasbourg, France, and Université de Haute Alsace, Mulhouse, France*
[20]*Institut de Physique Nucléaire de Lyon, IN2P3-CNRS, Université Claude Bernard, Villeurbanne, France*
[21]*III. Physikalisches Institut A, RWTH Aachen, Aachen, Germany*
[22]*Physikalisches Institut, Universität Bonn, Bonn, Germany*
[23]*Physikalisches Institut, Universität Freiburg, Freiburg, Germany*
[24]*Institut für Physik, Universität Mainz, Mainz, Germany*
[25]*Ludwig-Maximilians-Universität München, München, Germany*
[26]*Fachbereich Physik, University of Wuppertal, Wuppertal, Germany*
[27]*Panjab University, Chandigarh, India*

[28]Delhi University, Delhi, India
[29]Tata Institute of Fundamental Research, Mumbai, India
[30]University College Dublin, Dublin, Ireland
[31]Korea Detector Laboratory, Korea University, Seoul, Korea
[32]SungKyunKwan University, Suwon, Korea
[33]CINVESTAV, Mexico City, Mexico
[34]FOM-Institute NIKHEF and University of Amsterdam/NIKHEF, Amsterdam, The Netherlands
[35]Radboud University Nijmegen/NIKHEF, Nijmegen, The Netherlands
[36]Joint Institute for Nuclear Research, Dubna, Russia
[37]Institute for Theoretical and Experimental Physics, Moscow, Russia
[38]Moscow State University, Moscow, Russia
[39]Institute for High Energy Physics, Protvino, Russia
[40]Petersburg Nuclear Physics Institute, St. Petersburg, Russia
[41]Lund University, Lund, Sweden, Royal Institute of Technology and Stockholm University, Stockholm, Sweden, and Uppsala University, Uppsala, Sweden
[42]Physik Institut der Universität Zürich, Zürich, Switzerland
[43]Lancaster University, Lancaster, United Kingdom
[44]Imperial College, London, United Kingdom
[45]University of Manchester, Manchester, United Kingdom
[46]University of Arizona, Tucson, Arizona 85721, USA
[47]Lawrence Berkeley National Laboratory and University of California, Berkeley, California 94720, USA
[48]California State University, Fresno, California 93740, USA
[49]University of California, Riverside, California 92521, USA
[50]Florida State University, Tallahassee, Florida 32306, USA
[51]Fermi National Accelerator Laboratory, Batavia, Illinois 60510, USA
[52]University of Illinois at Chicago, Chicago, Illinois 60607, USA
[53]Northern Illinois University, DeKalb, Illinois 60115, USA
[54]Northwestern University, Evanston, Illinois 60208, USA
[55]Indiana University, Bloomington, Indiana 47405, USA
[56]University of Notre Dame, Notre Dame, Indiana 46556, USA
[57]Purdue University Calumet, Hammond, Indiana 46323, USA
[58]Iowa State University, Ames, Iowa 50011, USA
[59]University of Kansas, Lawrence, Kansas 66045, USA
[60]Kansas State University, Manhattan, Kansas 66506, USA
[61]Louisiana Tech University, Ruston, Louisiana 71272, USA
[62]University of Maryland, College Park, Maryland 20742, USA
[63]Boston University, Boston, Massachusetts 02215, USA
[64]Northeastern University, Boston, Massachusetts 02115, USA
[65]University of Michigan, Ann Arbor, Michigan 48109, USA
[66]Michigan State University, East Lansing, Michigan 48824, USA
[67]University of Mississippi, University, Mississippi 38677, USA
[68]University of Nebraska, Lincoln, Nebraska 68588, USA
[69]Princeton University, Princeton, New Jersey 08544, USA
[70]State University of New York, Buffalo, New York 14260, USA
[71]Columbia University, New York, New York 10027, USA
[72]University of Rochester, Rochester, New York 14627, USA
[73]State University of New York, Stony Brook, New York 11794, USA
[74]Brookhaven National Laboratory, Upton, New York 11973, USA
[75]Langston University, Langston, Oklahoma 73050, USA
[76]University of Oklahoma, Norman, Oklahoma 73019, USA
[77]Oklahoma State University, Stillwater, Oklahoma 74078, USA
[78]Brown University, Providence, Rhode Island 02912, USA
[79]University of Texas, Arlington, Texas 76019, USA
[80]Southern Methodist University, Dallas, Texas 75275, USA
[81]Rice University, Houston, Texas 77005, USA
[82]University of Virginia, Charlottesville, Virginia 22901, USA
[83]University of Washington, Seattle, Washington 98195, USA

(Dated: submitted to PRL on 15 March 2006; published 14 July 2006)

We report results of a study of the B_s^0 oscillation frequency using a large sample of B_s^0 semileptonic decays corresponding to approximately 1 fb^{-1} of integrated luminosity collected by the DØ experiment at the Fermilab Tevatron Collider in 2002–2006. The amplitude method gives a lower limit on the B_s^0 oscillation frequency at 14.8 ps^{-1} at the 95% C.L. At $\Delta m_s = 19$ ps^{-1}, the amplitude

deviates from the hypothesis $\mathcal{A} = 0$ ($\mathcal{A} = 1$) by 2.5 (1.6) standard deviations, corresponding to a two-sided C.L. of 1% (10%). A likelihood scan over the oscillation frequency, Δm_s, gives a most probable value of 19 ps^{-1} and a range of $17 < \Delta m_s < 21$ ps^{-1} at the 90% C.L., assuming Gaussian uncertainties. This is the first direct two-sided bound measured by a single experiment. If Δm_s lies above 22 ps^{-1}, then the probability that it would produce a likelihood minimum similar to the one observed in the interval $16 < \Delta m_s < 22$ ps^{-1} is $(5.0 \pm 0.3)\%$.

Measurements of flavor oscillations in the B_d^0 and B_s^0 systems provide important constraints on the CKM unitarity triangle and the source of CP violation in the standard model (SM) [1]. The phenomenon of B_d^0 oscillations is well established [2], with a precisely measured oscillation frequency Δm_d. In the SM, this parameter is proportional to the combination $|V_{tb}^* V_{td}|^2$ of CKM matrix elements. Since the matrix element V_{ts} is larger than V_{td}, the expected frequency Δm_s is higher. As a result, B_s^0 oscillations have not been observed by any previous experiment and the current 95% C.L. lower limit on Δm_s is 16.6 ps^{-1} [2]. A measurement of Δm_s would yield the ratio $|V_{ts}/V_{td}|$, which has a smaller uncertainty than $|V_{td}|$ alone due to the cancellation of certain theory uncertainties. If the SM is correct, and if current limits on B_s^0 oscillations are not included, then global fits to the unitarity triangle favor $\Delta m_s = 20.9^{+4.5}_{-4.2}$ ps^{-1} [3] or $\Delta m_s = 21.2 \pm 3.2$ ps^{-1} [4].

In this Letter, we present a study of B_s^0-$\bar{B}_s^0$ oscillations carried out using semileptonic $B_s^0 \rightarrow \mu^+ D_s^- X$ decays [5] collected by the DØ experiment at Fermilab in $p\bar{p}$ collisions at $\sqrt{s} = 1.96$ TeV. In the B_s^0-$\bar{B}_s^0$ system there are two mass eigenstates, the heavier (lighter) one having mass M_H (M_L) and decay width Γ_H (Γ_L). Denoting $\Delta m_s = M_H - M_L$, $\Delta \Gamma_s = \Gamma_L - \Gamma_H$, $\Gamma_s = (\Gamma_L + \Gamma_H)/2$, the time-dependent probability P that an initial B_s^0 decays at time t as $B_s^0 \rightarrow \mu^+ X$ (P^{nos}) or $\bar{B}_s^0 \rightarrow \mu^- X$ (P^{osc}) is given by $P^{\mathrm{nos/osc}} = e^{-\Gamma_s t}(1 \pm \cos \Delta m_s t)/2$, assuming that $\Delta \Gamma_s / \Gamma_s$ is small and neglecting CP violation. Flavor tagging a b ($\bar{b}$) on the opposite side to the signal meson establishes the signal meson as a B_s^0 ($\bar{B}_s^0$) at time $t = 0$.

The DØ detector is described in detail elsewhere [6]. Charged particles are reconstructed using the central tracking system which consists of a silicon microstrip tracker (SMT) and a central fiber tracker (CFT), both located within a 2-T superconducting solenoidal magnet. Electrons are identified by the preshower and liquid-argon/uranium calorimeter. Muons are identified by the muon system which consists of a layer of tracking detectors and scintillation trigger counters in front of 1.8-T iron toroids, followed by two similar layers after the toroids [7].

No explicit trigger requirement was made, although most of the sample was collected with single muon triggers. The decay chain $B_s^0 \rightarrow \mu^+ D_s^- X$, $D_s^- \rightarrow \phi \pi^-$, $\phi \rightarrow K^+ K^-$ was then reconstructed. The charged tracks were required to have signals in both the CFT and SMT. Muons were required to have transverse momentum $p_T(\mu^+) > 2$ GeV/c and momentum $p(\mu^+) > 3$ GeV/c, and to have measurements in at least two layers of the muon system. All charged tracks in the event were clustered into jets [8], and the D_s^- candidate was reconstructed from three tracks found in the same jet as the reconstructed muon. Oppositely charged particles with $p_T > 0.7$ GeV/c were assigned the kaon mass and were required to have an invariant mass $1.004 < M(K^+K^-) < 1.034$ GeV/c^2, consistent with that of a ϕ meson. The third track was required to have $p_T > 0.5$ GeV/c and charge opposite to that of the muon charge and was assigned the pion mass. The three tracks were required to form a common D_s^- vertex using the algorithm described in Ref. [9]. To reduce combinatorial background, the D_s^- vertex was required to have a positive displacement in the transverse plane, relative to the $p\bar{p}$ collision point (or primary vertex, PV), with at least 4σ significance. The cosine of the angle between the D_s^- momentum and the direction from the PV to the D_s^- vertex was required to be greater than 0.9. The trajectories of the muon and D_s^- candidates were required to originate from a common B_s^0 vertex, and the $\mu^+ D_s^-$ system was required to have an invariant mass between 2.6 and 5.4 GeV/c^2.

To further improve B_s^0 signal selection, a likelihood ratio method [10] was utilized. Using $M(K^+K^-\pi)$ sideband (B) and sideband-subtracted signal (S) distributions in the data, probability density functions (pdfs) were found for a number of discriminating variables: the helicity angle between the D_s^- and $K^\pm$ momenta in the ϕ center-of-mass frame, the isolation of the $\mu^+ D_s^-$ system, the χ^2 of the D_s^- vertex, the invariant masses $M(\mu^+ D_s^-)$ and $M(K^+K^-)$, and $p_T(K^+K^-)$. The final requirement on the combined selection likelihood ratio variable, y_{sel}, was chosen to maximize the predicted ratio $S/\sqrt{S+B}$. The total number of D_s^- candidates after these requirements was $N_{\mathrm{tot}} = 26{,}710 \pm 556\,(\mathrm{stat})$, as shown in Fig. 1(a).

The performance of the opposite-side flavor tagger (OST) [11] is characterized by the efficiency $\epsilon = N_{\mathrm{tag}}/N_{\mathrm{tot}}$, where N_{tag} is the number of tagged B_s^0 mesons; tag purity η_s, defined as $\eta_s = N_{\mathrm{cor}}/N_{\mathrm{tag}}$, where N_{cor} is the number of B_s^0 mesons with correct flavor identification; and the dilution $\mathcal{D}$, related to purity as $\mathcal{D} \equiv 2\eta_s - 1$. Again, a likelihood ratio method was used. In the construction of the flavor discriminating variables $x_1, ..., x_n$ for each event, an object, either a lepton ℓ
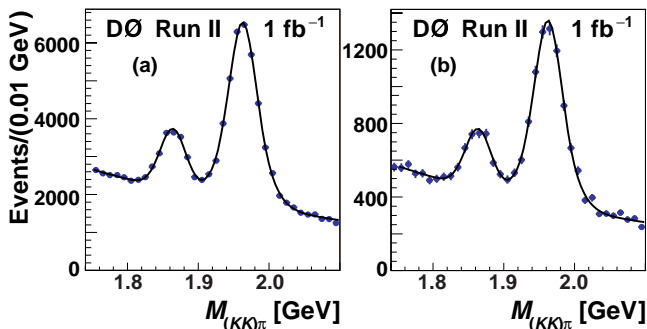
FIG. 1: $(K^+K^-)\pi^-$ invariant mass distribution for (a) the untagged B_s^0 sample, and (b) for candidates that have been flavor-tagged. The left and right peaks correspond to μ^+D^- and $\mu^+D_s^-$ candidates, respectively. The curve is a result of fitting a signal plus background model to the data.

(electron or muon) or a reconstructed secondary vertex (SV), was defined to be on the opposite side from the B_s^0 meson if it satisfied $\cos\varphi(\vec{p}_\ell \text{ or SV}, \vec{p}_B) < 0.8$, where $\vec{p}_B$ is the reconstructed three-momentum of the B_s^0 meson, and φ is the azimuthal angle about the beam axis. A lepton jet charge was formed as $Q_J^\ell = \sum_i q^i p_T^i / \sum_i p_T^i$, where all charged particles are summed, including the lepton, inside a cone of $\Delta R = \sqrt{(\Delta\varphi)^2 + (\Delta\eta)^2} < 0.5$ centered on the lepton. The SV charge was defined as $Q_{\rm SV} = \sum_i (q^i p_L^i)^{0.6} / \sum_i (p_L^i)^{0.6}$, where all charged particles associated with the SV are summed, and p_L^i is the longitudinal momentum of track i with respect to the direction of the SV momentum. Finally, event charge is defined as $Q_{\rm EV} = \sum_i q^i p_T^i / \sum_i p_T^i$, where the sum is over all tracks with $p_T > 0.5$ GeV/c outside a cone of $\Delta R > 1.5$ centered on the B_s^0 direction. The pdf of each discriminating variable was found for b and $\bar{b}$ quarks using a large data sample of $B^+ \to \mu^+\nu\bar{D}^0$ events where the initial state is known from the charge of the decay muon.

For an initial b ($\bar{b}$) quark, the pdf for a given variable x_i is denoted $f_i^b(x_i)$ ($f_i^{\bar{b}}(x_i)$), and the combined tagging variable is defined as $d_{\rm tag} = (1-z)/(1+z)$, where $z = \prod_{i=1}^n (f_i^{\bar{b}}(x_i)/f_i^b(x_i))$. The variable $d_{\rm tag}$ varies between -1 and 1. An event with $d_{\rm tag} > 0$ (< 0) is tagged as a b ($\bar{b}$) quark.

The OST purity was determined from large samples of $B^+ \to \mu^+\bar{D}^0 X$ (non-oscillating) and $B_d^0 \to \mu^+ D^{*-} X$ (slowly oscillating) semileptonic candidates. An average value of $\epsilon\mathcal{D}^2 = [2.48 \pm 0.21\,(\text{stat})^{+0.08}_{-0.06}\,(\text{syst})]\%$ was obtained [11]. The estimated event-by-event dilution as a function of $|d_{\rm tag}|$ was determined by measuring $\mathcal{D}$ in bins of $|d_{\rm tag}|$ and parametrizing with a third-order polynomial for $|d_{\rm tag}| < 0.6$. For $|d_{\rm tag}| > 0.6$, $\mathcal{D}$ is fixed to 0.6.

The OST was applied to the $B_s^0 \to \mu^+ D_s^- X$ data sample, yielding $N_{\rm tag} = 5601 \pm 102\,(\text{stat})$ candidates having an identified initial state flavor, as shown in Fig. 1(b). The tagging efficiency was $(20.9 \pm 0.7)\%$.

After flavor tagging, the proper decay time of candidates is needed; however, the undetected neutrino and other missing particles in the semileptonic B_s^0 decay prevent a precise determination of the meson's momentum and Lorentz boost. This represents an important contribution to the smearing of the proper decay length in semileptonic decays, in addition to the resolution effects. A correction factor K was estimated from a Monte Carlo (MC) simulation by finding the distribution of $K = p_T(\mu^+ D_s^-)/p_T(B)$ for a given decay channel in bins of $M(\mu^+ D_s^-)$. The proper decay length of each B_s^0 meson is then $ct(B_s^0) = l_M K$, where $l_M = M(B_s^0) \cdot (\vec{L}_T \cdot \vec{p}_T(\mu^+ D_s^-))/(p_T(\mu^+ D_s^-))^2$ is the measured visible proper decay length (VPDL), $\vec{L}_T$ is the vector from the PV to the B_s^0 decay vertex in the transverse plane and $M(B_s^0) = 5.3696$ GeV/c^2 [1].

All flavor-tagged events with $1.72 < M(K^+K^-\pi^-) < 2.22$ GeV/c^2 were used in an unbinned fitting procedure. The likelihood, $\mathcal{L}$, for an event to arise from a specific source in the sample depends event-by-event on l_M, its uncertainty σ_{l_M}, the invariant mass of the candidate $M(K^+K^-\pi^-)$, the predicted dilution $\mathcal{D}(d_{\rm tag})$, and the selection variable $y_{\rm sel}$. The pdfs for σ_{l_M}, $M(K^+K^-\pi^-)$, $\mathcal{D}(d_{\rm tag})$ and $y_{\rm sel}$ were determined from data. Four sources were considered: the signal $\mu^+ D_s^- (\to \phi\pi^-)$; the accompanying peak due to $\mu^+ D^- (\to \phi\pi^-)$; a small (less than 1%) reflection due to $\mu^+ D^- (\to K^+\pi^-\pi^-)$, where the kaon mass is misassigned to one of the pions; and combinatorial background. The total fractions of the first two categories were determined from the mass fit of Fig. 1(b).

The $\mu^+ D_s^-$ signal sample is composed mostly of B_s^0 mesons with some contributions from B_d^0 and B^+ mesons. Contributions of b baryons to the sample were estimated to be small and were neglected. The data were divided into subsamples with and without oscillation as determined by the OST. The distribution of the VPDL l for non-oscillated and oscillated cases was modeled appropriately for each type of B meson, e.g., for B_s^0:

$$p_s^{\rm nos/osc}(l, K, d_{\rm tag}) = \qquad\qquad (1)$$
$$\frac{K}{c\tau_{B_s^0}} \exp(-\frac{Kl}{c\tau_{B_s^0}})[1 \pm \mathcal{D}(d_{\rm tag})\cos(\Delta m_s \cdot Kl/c)]/2.$$

The world averages [1] of $\tau_{B_d^0}$, τ_{B^+}, and Δm_d were used as inputs to the fit. The lifetime, $\tau_{B_s^0}$, was allowed to float in the fit. In the amplitude and likelihood scans described below, $\tau_{B_s^0}$ was fixed to this fitted value, which agrees with expectations.

The total VPDL pdf for the $\mu^+ D_s^-$ signal is then the sum over all decay channels, including branching fractions, that yield the D_s^- mass peak. The $B_s^0 \to \mu^+ D_s^- X$ signal modes (including D_s^{*-}, D_{s0}^{*-}, and $D_{s1}^{'-}$; and μ^+ originating from τ^+ decay) comprise $(85.6 \pm 3.3)\%$ of our sample, as determined from a MC simulation which included the PYTHIA generator v6.2 [12] interfaced with the EVTGEN decay package [13], followed by full

GEANT v3.15 [14] modeling of the detector response and event reconstruction. Other backgrounds considered were decays via $B_s^0 \to D_{(s)}^+ D_s^- X$ and $\bar{B}_d^0, B^- \to DD_s^-$, followed by $D_{(s)}^+ \to \mu^+ X$, with a real D_s^- reconstructed in the peak and an associated real μ^+. Another background taken into account occurs when the D_s^- meson originates from one b or c quark and the muon arises from another quark. This background peaks around the PV (peaking backgrounds). The uncertainty in each channel covers possible trigger efficiency biases. Translation from the true VPDL, l, to the measured l_M for a given channel, is achieved by a convolution of the VPDL detector resolution, of K factors over each normalized distribution, and by including the reconstruction efficiency as a function of VPDL. The lifetime-dependent efficiency was found for each channel using MC simulations and, as a cross check, the efficiency was also determined from the data by fixing $\tau_{B_s^0}$ and fitting for the functional form of the efficiency. The shape of the VPDL distribution for peaking backgrounds was found from MC simulation, and the fraction from this source was allowed to float in the fit.

The VPDL uncertainty was determined from the vertex fit using track parameters and their uncertainties. To account for possible mismodeling of these uncertainties, resolution scale factors were introduced as determined by examining the pull distribution of the vertex positions of a sample of $J/\psi \to \mu^+ \mu^-$ decays. Using these scale factors, the convolving function for the VPDL resolution was the sum of two Gaussians with widths (fractions) of $0.998\sigma_{l_M}$ (72%) and $1.775\sigma_{l_M}$ (28%). A cross check was performed using a MC simulation with tracking errors tuned according to the procedure described in [15]. The 7% variation of scale factors found in this cross check was used to estimate systematic uncertainties due to decay length resolution.

Several contributions to the combinatorial backgrounds that have different VPDL distributions were considered. True prompt background was modeled with a Gaussian function with a separate scale factor on the width; background due to fake vertices around the PV was modeled with another Gaussian function; and long-lived background was modeled with an exponential function convoluted with the resolution, including a component oscillating with a frequency of Δm_d. The unbinned fit of the total tagged sample was used to determine the various fractions of signal and backgrounds and the background VPDL parametrizations.

Figure 2 shows the value of $-\Delta \log \mathcal{L}$ as a function of Δm_s, indicating a favored value of 19 ps^{-1}, while variation of $-\log \mathcal{L}$ from the minimum indicates an oscillation frequency of $17 < \Delta m_s < 21$ ps^{-1} at the 90% C.L. The uncertainties are approximately Gaussian inside this interval. The plateau of the likelihood curve shows the region where we do not have sufficient resolution to measure an oscillation, and if the true value of
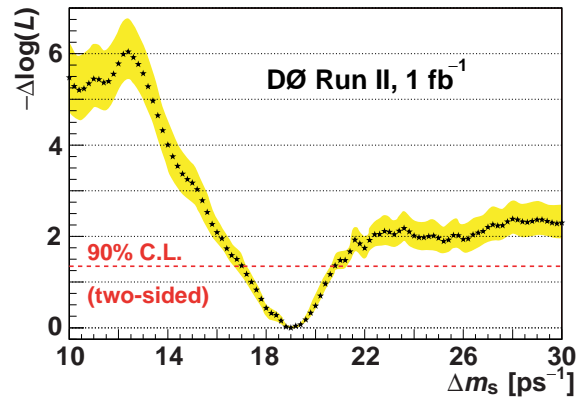

FIG. 2: Value of $-\Delta \log \mathcal{L}$ as a function of Δm_s. Star symbols do not include systematic uncertainties, and the shaded band represents the envelope of all $\log \mathcal{L}$ scan curves due to different systematic uncertainties.

$\Delta m_s > 22$ ps^{-1}, our measured confidence interval does not make any statement about the frequency. Using 100 parametrized MC samples with similar statistics, VPDL resolution, overall tagging performance, and sample composition of the data sample, it was determined that for a true value of $\Delta m_s = 19$ ps^{-1}, the probability was 15% for measuring a value in the range $16 < \Delta m_s < 22$ ps^{-1} with a $-\Delta \log \mathcal{L}$ lower by at least 1.9 than the corresponding value at $\Delta m_s = 25$ ps^{-1}.

The amplitude method [16] was also used. Equation 1 was modified to include the oscillation amplitude $\mathcal{A}$ as an additional coefficient on the $\cos(\Delta m_s \cdot Kl/c)$ term. The unbinned fit was repeated for fixed input values of Δm_s and the fitted value of $\mathcal{A}$ and its uncertainty $\sigma_{\mathcal{A}}$ found for each step, as shown in Fig. 3. At $\Delta m_s = 19$ ps^{-1} the measured data point deviates from the hypothesis $\mathcal{A} = 0$ ($\mathcal{A} = 1$) by 2.5 (1.6) standard deviations, corresponding to a two-sided C.L. of 1% (10%), and is in agreement with the likelihood results. In the presence of a signal, however, it is more difficult to define a confidence interval using the amplitude than by examining the $-\Delta \log \mathcal{L}$ curve. Since, on average, these two methods give the same results, we chose to quantify our Δm_s interval using the likelihood curve.

Systematic uncertainties were addressed by varying inputs, cut requirements, branching ratios, and pdf modeling. The branching ratios were varied within known uncertainties [1] and large variations were taken for those not yet measured. The K-factor distributions were varied within uncertainties, using measured (or smoothed) instead of generated momenta in the MC simulation. The fractions of peaking and combinatorial backgrounds were varied within uncertainties. Uncertainties in the reflection contribution were considered. The functional form to determine the dilution $\mathcal{D}(d_{tag})$ was varied. The lifetime $\tau_{B_s^0}$ was fixed to its world average value, and $\Delta\Gamma_s$ was allowed to be non-zero. The scale factors on the sig-
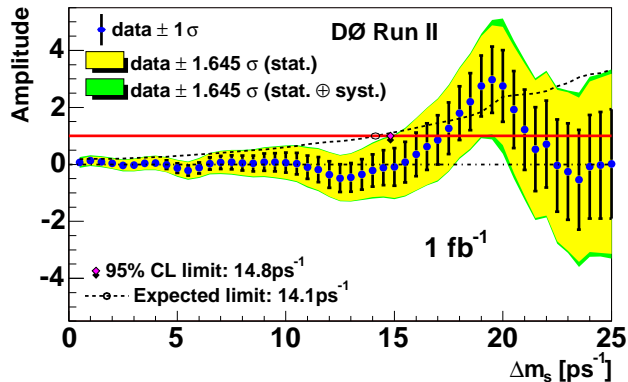
FIG. 3: B_s^0 oscillation amplitude as a function of oscillation frequency, Δm_s. The solid line shows the $\mathcal{A} = 1$ axis for reference. The dashed line shows the expected limit including both statistical and systematic uncertainties.

nal and background resolutions were varied within uncertainties, and typically generated the largest systematic uncertainty in the region of interest. A separate scan of $-\Delta \log \mathcal{L}$ was taken for each variation, and the envelope of all such curves is indicated as the band in Fig. 2. The same systematic uncertainties were considered for the amplitude method using the procedure of Ref. [16], and, when added in quadrature with the statistical uncertainties, represent a small effect, as shown in Fig. 3. Taking these systematic uncertainties into account, we obtain from the amplitude method an expected limit of 14.1 ps^{-1} and an observed lower limit of $\Delta m_s > 14.8$ ps^{-1} at the 95% C.L., consistent with the likelihood scan.

The probability that B_s^0-$\bar{B}_s^0$ oscillations with the true value of $\Delta m_s > 22$ ps^{-1} would give a $-\Delta \log \mathcal{L}$ minimum in the range $16 < \Delta m_s < 22$ ps^{-1} with a depth of more than 1.7 with respect to the $-\Delta \log \mathcal{L}$ value at $\Delta m_s = 25$ ps^{-1}, corresponding to our observation including systematic uncertainties, was found to be $(5.0\pm0.3)\%$. This range of Δm_s was chosen to encompass the world average lower limit and the edge of our sensitive region. To determine this probability, an ensemble test using the data sample was performed by randomly assigning a flavor to each candidate while retaining all its other information, effectively simulating a B_s^0 oscillation with an infinite frequency. Similar probabilities were found using ensembles of parametrized MC events.

In summary, a study of B_s^0-$\bar{B}_s^0$ oscillations was performed using $B_s^0 \to \mu^+ D_s^- X$ decays, where $D_s^- \to \phi \pi^-$ and $\phi \to K^+K^-$, an opposite-side flavor tagging algorithm, and an unbinned likelihood fit. The amplitude method gives an expected limit of 14.1 ps^{-1} and an observed lower limit of $\Delta m_s > 14.8$ ps^{-1} at the 95% C.L. At $\Delta m_s = 19$ ps^{-1}, the amplitude method yields a result that deviates from the hypothesis $\mathcal{A} = 0$ ($\mathcal{A} = 1$)

by 2.5 (1.6) standard deviations, corresponding to a two-sided C.L. of 1% (10%). The likelihood curve is well behaved near a preferred value of 19 ps^{-1} with a 90% C.L. interval of $17 < \Delta m_s < 21$ ps^{-1}, assuming Gaussian uncertainties. The lower edge of the confidence level interval is near the world average 95% C.L. lower limit $\Delta m_s > 16.6$ ps^{-1} [2]. Ensemble tests indicate that if Δm_s lies above the sensitive region, i.e., above approximately 22 ps^{-1}, there is a $(5.0\pm0.3)\%$ probability that it would produce a likelihood minimum similar to the one observed in the interval $16 < \Delta m_s < 22$ ps^{-1}. This is the first report of a direct two-sided bound measured by a single experiment on the B_s^0 oscillation frequency.

[*] On leave from IEP SAS Kosice, Slovakia.
[†] Visitor from Helsinki Institute of Physics, Helsinki, Finland.

[1] S. Eidelman et al., Phys. Lett. B **592**, 1 (2004).
[2] E. Barberio et al. (Heavy Flavor Averaging Group), hep-ex/0603003. Note that we take $\hbar = c = 1$, hence the units on Δm_s.
[3] J. Charles et al. (CKMfitter Group), Eur. Phys. J. **C41**, 1 (2005).
[4] M. Bona et al. (UTfit Collaboration), J. High Energy Phys. **07**(2005) 028.
[5] Charge conjugate states are assumed throughout.
[6] V. Abazov et al. (DØ Collaboration), physics/0507191 [Nucl. Instrum. Methods Phys. Res. Sect. A (to be published)].
[7] V.M. Abazov et al., Nucl. Instrum. Methods Phys. Res. Sect. A **552**, 372 (2005).
[8] S. Catani et al., Phys. Lett. B **269**, 432 (1991), "Durham" jets with the p_T cut-off parameter set at 15 GeV/c.
[9] J. Abdallah et al. (DELPHI Collaboration), Eur. Phys. J. C **32**, 185 (2004).
[10] G. Borisov, Nucl. Instrum. Methods Phys. Res. Sect. A **417**, 384 (1998).
[11] V. Abazov et al. (DØ Collaboration), Phys. Rev. D (to be published); DØ Note 5029, available from http://www-d0.fnal.gov/Run2Physics/WWW/results/prelim/B/B32/.

[12] T. Sjöstrand *et al.*, Comput. Phys. Commun. **135**, 238 (2001).

[13] D.J. Lange, Nucl. Instrum. Methods Phys. Res. Sect. A **462**, 152 (2001).

[14] R. Brun and F. Carminati, CERN Program Library Long Writeup W5013 (unpublished).

[15] G. Borisov and C. Mariotti, Nucl. Instrum. Methods Phys. Res. Sect. A **372**, 181 (1996).

[16] H.G. Moser and A. Roussarie, Nucl. Instrum. Methods Phys. Res. Sect. A **384**, 491 (1997).